Separation and Purification Technology 338 (2024) 126457

Contents lists available at ScienceDirect

Separation and Purification Technology

journal homepage: www.elsevier.com/locate/seppur

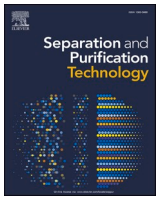

Rational design of a donor-acceptor structured poly(3-bromothiophene) modified g-C_3N_4 for enhanced photocatalytic degradation of 2-mercaptobenzothiazole

Yao Huang [a], Xuefeng Hu [a,*], Chuanyi Wang [a], Detlef Bahnemann [a,b]

[a] School of Environmental Science and Engineering, Shaanxi University of Science and Technology, Weiyang District, Xi'an 710021, China
[b] Laboratory of Photoactive Nanocomposite Materials, Saint-Petersburg State University, Ulyanovskaya Str. 1, Peterhof, Saint-Petersburg 198504, Russia

ARTICLE INFO

Keywords:
g-C_3N_4
Donor-acceptor structure
Conjugated polymer
Visible-light irradiation
Poly(3-bromothiophene)

ABSTRACT

Donor-acceptor (D-A) structure has gained momentous attention due to its controllable optical band gap and impressive carrier separation performance. The intramolecular charge transfer within photocatalysts could be modulated by constructing a D-A structure, thereby enhancing their performance in degrading pollutants. In our recent research, using poly(3-bromothiophene) (PTh-Br) and dicyandiamide (DCD) as precursors, a series of D-A structures (CN-PTh-Br(x)) based on polythiophene donors and carbon nitride acceptors were obtained by one-pot synthesis for first-time. The density functional theory calculations further demonstrate that PTh-Br segment (an electron donor) donates electrons to tri-s-triazine rings (an electron acceptor). The introduction of electron-rich polythiophene groups and electron-withdrawing Br atoms on carbon nitride skeleton can propel the transfer and separation of holes and electrons. Moreover, the polythiophene groups with high conjugation length can optimize the optical absorption of CN-PTh-Br(x) at 450–600 nm, thus markedly heightening the visible-light utilization efficiency of the materials. The photocatalytic performance of CN-PTh-Br(x) was assessed through the photodegradation of 2-mercaptobenzothiazole (MBT) under visible-light illumination. The photodegradation performance of CN-PTh-Br(0.5) stood out among all the samples, demonstrating a remarkable ability to remove 99.8% of MBT within 45 min.

1. Introduction

Photocatalysis has garnered major attention due to the capacity to utilize solar energy for the removal of harmful pollutants. At the heart of photocatalysis lies the semiconductor photocatalyst, which exhibits redox capabilities in the presence of light. Nevertheless, the limited exploitation of visible light and the rapid recombination of electrons and holes pose significant challenges to the functional implementation of photocatalysts.[1–9] Consequently, numerous researchers have focused their efforts on addressing these shortcomings in order to achieve efficient and safe practical applications.

Graphitized carbon nitride (g-C_3N_4) is a two-dimensional polymer semiconductor that can act as a photocatalyst with excellent photocatalytic performance.[10] It can be obtained by heating precursors such as cyanamide[11,12], dicyandiamide[13], urea[14], and melamine[15]. However, the photocatalytic effectiveness of g-C_3N_4 is constrained by the low visible-light absorption and the rapid electron-hole pairs recombination. Consequently, a variety of modification techniques have been developed to boost its photocatalytic performance, including surface modification[16–19], metal or non-metal doping[20–23], and heterojunctions creation[24–27]. Nevertheless, given the constraints of traditional techniques, the development of novel modification strategies continues to be crucial. Creating a donor–acceptor (D-A) structure triggers an internal electric field, which aids in holes and electrons generation. The electron affinity difference enhances intramolecular charge transfer, resulting in electron transfer from the electron donor segment to the electron acceptor segment.[28]

In recent years, numerous researches have explored the rational design of D-A structures based on g-C_3N_4. Che et al.[29] conducted a study where they prepared an innovative D-A structure with high photocatalytic activity by thermal copolymerisation. The experimental results demonstrated that the resulting porous D-A structured photocatalysts not only enhanced the utilization of light but also facilitated the migration of carriers due to the introduction of formaldehyde

* Corresponding author.
E-mail address: huxuefeng@sust.edu.cn (X. Hu).

https://doi.org/10.1016/j.seppur.2024.126457
Received 13 November 2023; Received in revised form 9 January 2024; Accepted 16 January 2024
Available online 22 January 2024

resin in the photocatalyst structure. Wu et al.[30] used two materials as precursors for synthesizing a variety of D-A structures based on g-C_3N_4, which expanded the visible-light capturing capability and accelerated the photogenerated electron and hole separation. In all the cases mentioned above, electron acceptor segments that can facilitate the efficient transfer of electrons were introduced into the g-C_3N_4 structure. It is well known that electron reduction on the photocatalyst LUMO is the primary source of free radicals in photocatalysis. This implies that introducing electron-acceptor fragments into the photocatalyst framework reduces its LUMO energy, thereby hindering the production of active free radicals.[31] Therefore, g-C_3N_4 acts as an electron-acceptor, and the introduction of an electron-donor fragment into its skeleton will facilitate the continuous transfer of electrons from electron donor to electron acceptor, thus intensifying the separation of holes and electrons.

Conjugated polymer is a kind of semiconductor material with a designable structure, high chemical stability, and strong optical trapping ability, which has a wide application prospect.[32,33] Conjugated polymers such as polypyrrole[34,35], polyaniline[36], polythiophene [37–39], or polyvinylpyrrolidone[40] are combined with pre-prepared g-C_3N_4, and the resulting heterostructures have been shown to ameliorate the carrier mobility and visible light utilization of the prepared photocatalysts, thus achieving organic pollutant degradation and hydrogen production. Poly(3-bromothiophene) (PTh-Br) has a compact and stable structure with good environmental stability[41], but the modification of g-C_3N_4 with PTh-Br has not been reported.

In this study, PTh-Br was first prepared, and then PTh-Br and dicyandiamide (DCD) were used as precursors to obtain the D-A structured CN-PTh-Br(x) by thermal copolymerization. PTh-Br was chosen as the electron donor unit because of the electro-rich nature of the thiophene groups and the electron-absorbing nature of the Br atoms. The addition of PTh-Br narrows the band gap, improves the optical harvesting capacity, reduces the photogenerated carriers recombination, and boosts the photodegradation efficiency. A potential photocatalytic mechanism was proposed, and the photocatalytic activity and photodegradation durability of the prepared CN-PTh-Br(0.5) were investigated.

2. Materials and methods

2.1. Materials

3-Bromothiophene (Th-Br), trifluoroacetic acid (TFA), and boron trifluoride diethyl etherate (BFEE) were procured from Macklin (Shanghai, China). Sodium sulfate (Na_2SO_4) and Ethylenediaminetetraacetic acid disodium salt (EDTA-2Na) were purchased from Tianli (Tianjin, China). Dicyandiamide (DCD), *tert*-Butanol (TBA), L-Ascorbic acid, and methyl alcohol (MeOH) were provided from Damao (Tianjin, China). Absolute ethanol (EtOH) was acquired from Fuyu (Tianjin, China). 2-Mercaptobenzothiazole (MBT) was produced by Aladdin (Shanghai, China).

2.2. Methods

2.2.1. Preparation of poly(3-bromothiophene) (PTh-Br)

The electrochemical polymerization of monomer Th-Br was implemented using a tri-electrode system on an electrochemical workstation (Scheme S1). Two Pt sheets with a surface area of 1 cm^2 were utilized as both the working and counter electrodes for polymer production. A Pt wire with a radius of 0.25 mm was employed as the reference electrode. The electrolytic medium utilized was a mixture of TFA/BFEE in a 1:9 volumetric ratio containing 0.1 mol/L Th-Br. The procedure of electropolymerization was executed at a sustained potential of 0.7 V for a duration of 2 h. The residual solution was diluted with DI water and then subjected to three extractions with $CHCl_3$. The organic layers were then combined, dried, filtered, and evaporated to yield a polymer named PTh-Br. The gel permeation chromatography (GPC) measurements of obtained PTh-Br showed a number-average molecular weight (M_n) of 307806, a weight-average molecular weight (M_w) of 308461, and a polydispersity index (PDI) of 1.002.

2.2.2. Preparation of CN-PTh-Br(x) and CN

Thermal copolymerisation was carried out with PTh-Br and DCD as precursors (Scheme S2). DCD and PTh-Br were dissolved in methanol successively at 40 ℃, stirring at the above temperature for 30 min, drying at 60 ℃, and grinding for 30 min. The powdered mixture is then added to the ceramic crucible, which is subsequently covered and transferred to the muffle furnace. The mixture was progressively heated to 550 °C at a rate of 5 °C per minute, followed by continuous calcination at 550 °C for 4 h. The acquired catalysts were denoted as CN-PTh-Br(x) (x = 0.1, 0.3, 0.5, 0.7, and 1.0), respectively, where x% is the used weight ratio of PTh-Br to DCD. As a comparison, pristine CN catalyst was obtained by calcinating DCD using a similar procedure as mentioned above without PTh-Br. For the purpose of better investing solid-state nuclear magnetic resonance (ssNMR), the weight ratio of PTh-Br to DCD was increased to 30%, denoted as CN-PTh-Br(30).

2.3. Characterization

The detailed characterization is shown in Text S1.

2.4. Photocatalytic degradation experiments

2.4.1. Photodegradation of MBT

Using a CEL-HXF300 Xe-lamp equipped with a $\lambda \geq 420$ nm UV cut-off filter as the sole light source, the photocatalytic performance of each photocatalyst was assessed. In general, for a consistent ratio of photocatalyst to organic contaminant solution across the photocatalysis process, 20 mg of the acquired catalytic sample was scattered in 20 mL of MBT solution (20 mg/L). Before initiating the photodegradation trial, the suspension was agitated away from light for 30 min to attain the adsorption–desorption equilibrium. During the photocatalytic reaction, a 1.5 mL sample of the reaction mixture was periodically filtered and collected using a mixed cellulose ester filter head (0.22 μm in pore size) to entirely remove the photocatalyst particles from the sample. The concentration of the remaining MBT solution at each stage during photocatalytic degradation was measured by a Shimadzu LC-16 liquid chromatography. The calculation formulas of degradation efficiency and degradation reaction rate constant are shown in Text S2.

2.4.2. Cycle experiments

The reusability of CN-PTh-Br(0.5) was investigated by recycling experiments. The same CN-PTh-Br(0.5) sample was employed five times for the photocatalytic removal reaction of MBT. After the end of each reaction, the catalyst underwent a process of filtration, washing, and drying. Filtration was performed under vacuum, washing twice each involved alternating between DI water and EtOH, and drying was done at 60℃ for 2 h.

2.4.3. Radicals trapping experiments

To investigate the principal active species in the photocatalytic degradation of organic pollutants, we employed the radical quenching assay, which is accomplished by adding suitable scavengers during the photodegradation process. The applied scavengers in the process include L-Ascorbic acid, EDTA-2Na, and TBA, which were employed to neutralize superoxide radical ($\cdot O_2^-$), holes (h^+), and hydroxyl radical ($\cdot OH$), respectively. The concentration of each scavenger used in the solution was 5 mmol/L.

2.5. Photoelectric performance test

The electrochemical test was conducted on a CHI660E

electrochemical workstation using an electrolyte of 0.5 mol/L Na_2SO_4. In the aforementioned experiment, a one-chamber triple-electrode system was employed with a prepared photoelectrode sheet (working electrode), a platinum sheet (counter electrode), and a saturated calomel electrode (reference electrode). A CEL-HXF300 Xe-lamp equipped with $\lambda \geq 420$ nm UV cut-off filter is utilized as the light source. The preparation of the photoelectrode and the photoelectric performance test parameters are described in Text S3.

2.6. Computational details

The density-functional-theory (DFT) calculations were carried out by using Gaussian 16 software[42]. The molecular structures were built using GaussView 6.0.16 Program[43]. The B3LYP functions, the 6-311G (*d*, *p*) basis set, and the GD3BJ semi-classical approach for dispersion correction were used in all DFT calculations. The highest occupied molecular orbital (HOMO) and the lowest unoccupied molecular orbital (LUMO) of CN and CN-PTh-Br(0.5) were constructed, respectively.

3. Results and discussion

3.1. Characterization

The transmission emission microscope (TEM) and scanning electron microscope (SEM) were applied to detect the morphologies of the photocatalytic samples. Compared with the typical lamellar structures of CN in Fig. 1a-b, the sheet-like structures of CN-PTh-Br(0.5) in Fig. 1c-d become thinner and smaller. The formation of smaller flake structures may be due to the introduction of PTh-Br during the copolymerisation process resulting in the hindered bonding degree of the melon units. It is known that the ultrathin layered structure facilitates charge transfer and light absorption. Fig. 1e demonstrates that the elements C, N, S, and Br are dispersed on the surface of the sheet.

To gain further information on the chemical structures of the catalysts, a series of solid-state nuclear magnetic resonance (ssNMR) experiments were conducted. Fig. 2a-b shows the molecular structures of CN and CN-PTh-Br(30), respectively. ^{1}H ssNMR spectra of CN and CN-PTh-Br(30) are shown in Fig. 2c, and two strong and wide peaks can be observed, where the chemical shift of ~ 4.4 ppm represents the signal of residual water, and the chemical shift of ~ 9.0 ppm represents the signal of amino groups and aromatic heterocycle. The ratio of signal intensities of CN-PTh-Br(30) at ~ 9.0 ppm and ~ 4.4 ppm chemical shifts is greater than that of CN, due to the introduction of the polymer PTh-Br into the edge of the CN-PTh-Br(30) carbon nitride framework. Fig. 2d presents ^{13}C ssNMR spectra of CN and CN-PTh-Br(30), where the characteristic peaks of CN and CN-PTh-Br(30) include exocyclic carbon (C1) located at 164.3 ppm and endocyclic carbon (C2) located at 156.5 ppm.[44–46] These chemical shift assignments are consistent with previous reports. From Fig. 4d, a new weak peak located at ~ 128.9 ppm is on account of aromatic heterocycle C=C. This indicates that the carbon nitride framework is still maintained in CN-PTh-Br(30), while the PTh-Br structure has been successfully grafted onto the edges of the carbon nitride skeleton. The structures of CN and CN-PTh-Br(0.5) were further characterized by XRD (Fig. S1a), AFM (Fig. S1b), and ATR-FTIR (Fig. S2). It can be seen that the carbon nitride framework structure of CN-PTh-Br(0.5) remains essentially unchanged after the introduction of PTh-Br, which is consistent with the ssNMR results.

Subsequently, the specific Brunauer-Emmett-Teller (BET) surface area of CN and CN-PTh-Br(0.5) was examined by N_2 adsorption–desorption isotherms. As illustrated in Fig. 3, all catalyst samples exhibit type IV isotherms with H3 hysteresis loops, revealing the mesoporous structures.[47] As shown in Table S1, the BET surface area of CN-PTh-Br(0.5) is 9.14 $m^2\ g^{-1}$, which is slightly higher than that of CN (8.27 $m^2\ g^{-1}$). This increase can be attributed to the gases (HBr and NH_3) released by the introduction of PTh-Br during calcination.[48,49] Additionally, as the pore size and BET surface area increase, the exposure of the active sites to organic contaminants also increases, thereby achieving improved photocatalytic degradation performance.

From Fig. 4, the X-ray photoelectron spectroscopy (XPS) spectra of CN and CN-PTh-Br(0.5) are exhibited. The overall XPS survey spectra show little difference, which may be due to the insufficient addition of PTh-Br. Fig. 4a displays the full spectra of catalyst elements, and the elements C, N, and O are present in all catalysts.

In Fig. 4b, the high-resolution XPS spectra of C 1s in CN can be fitted to three peak components at 284.60 eV (C–C/C=C), 286.02 eV (C-NH_x), and 287.59 eV (N-C=N).[50] The relatively stronger peak at 284.60 eV in CN-PTh-Br(0.5) is due to the presence of aromatic heterocycles in PTh-Br. Fig. 4c shows high-resolution XPS spectra of N 1s, in which CN exhibits four peaks centered at 398.01 (C-N=C), 399.94 (N-$(C)_3$), 400.62 (C-N–H), and 403.91 eV (π-π*).[51] Notably, Remarkably, in CN-PTh-Br (0.5), the binding energy of the N-$(C)_3$ group (398.81 eV) shifts to a lower binding energy due to electron acquisition, and the relative

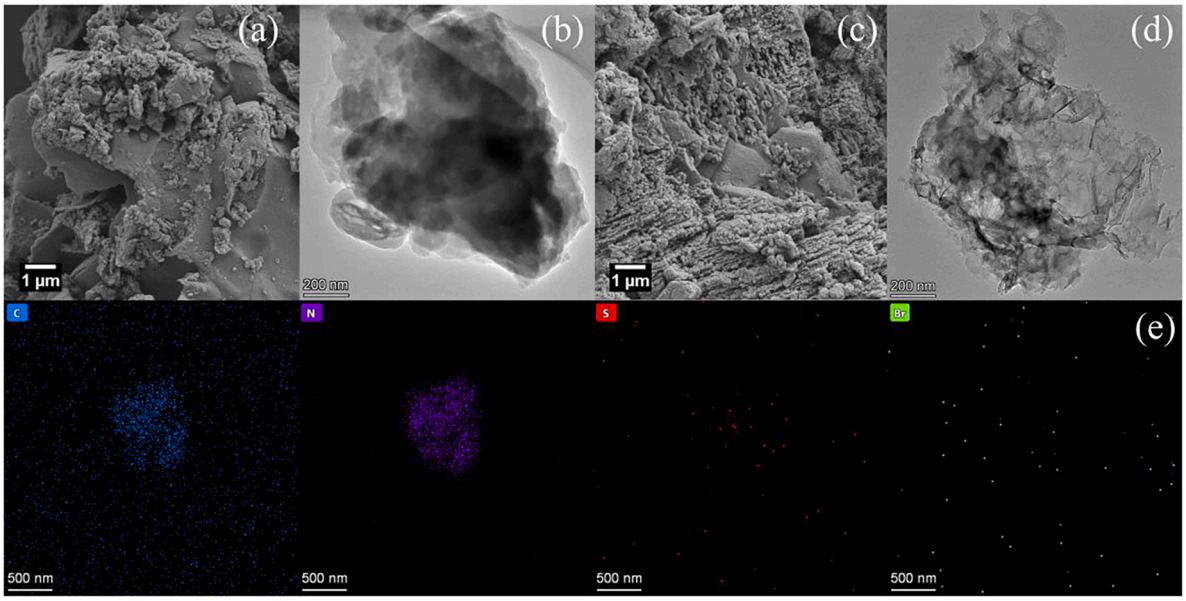

Fig. 1. (a) SEM and (b) TEM images of CN, (c) SEM and (d) TEM images of CN-PTh-Br(0.5), (e) elemental mapping images of CN-PTh-Br(0.5).

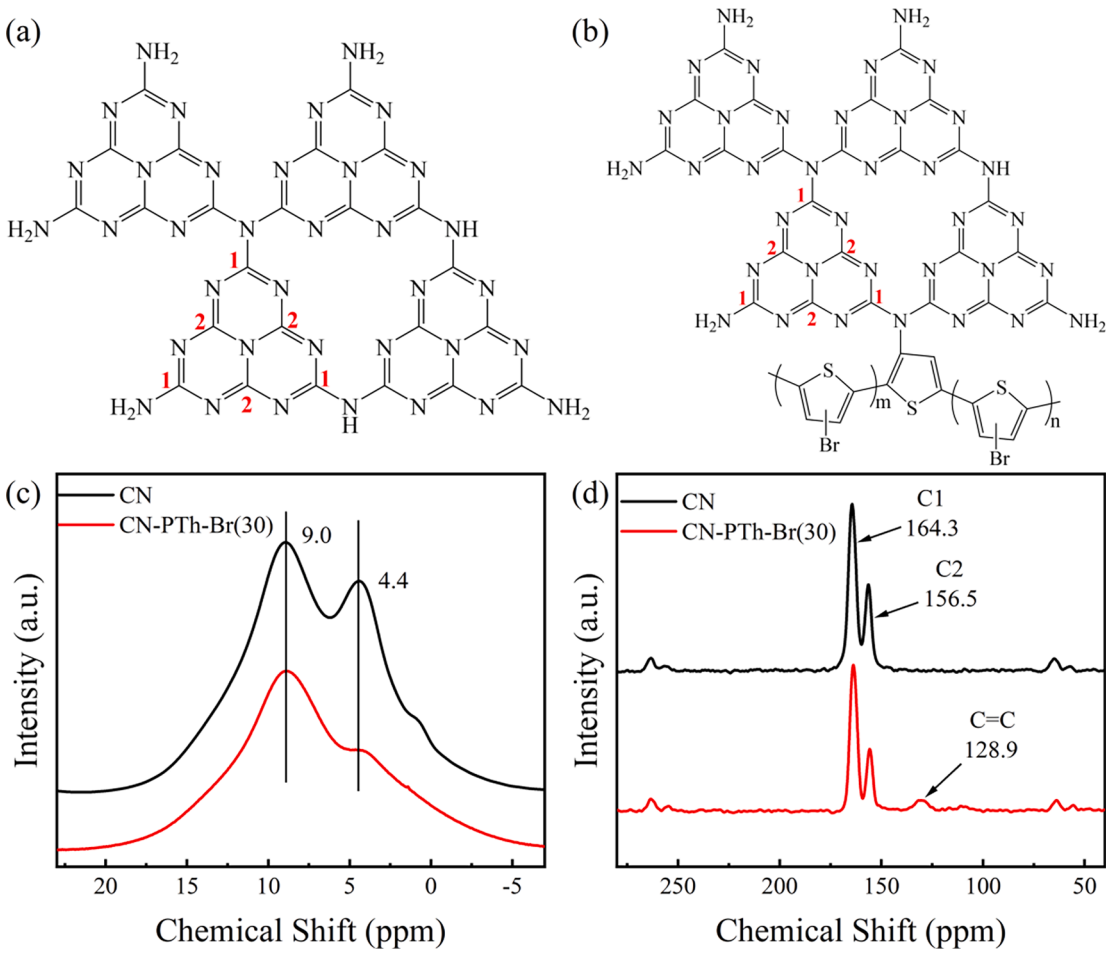

Fig. 2. The molecular structures of (a) CN and (b) CN-PTh-Br(30). (c) ^{1}H ssNMR spectra and (d) ^{13}C ssNMR spectra of CN and CN-PTh-Br(30).

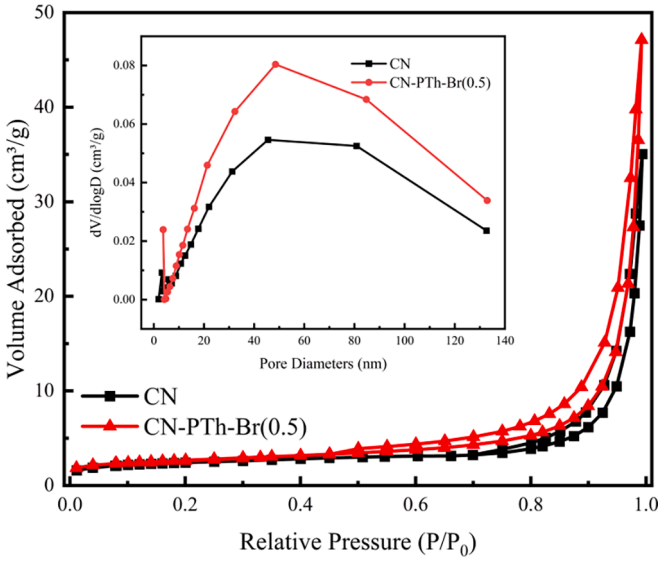

Fig. 3. The N_2 adsorption–desorption isotherms, and corresponding pore size distribution curves (inset) of CN and CN-PTh-Br(0.5).

enhancement of the peak of the N-$(C)_3$ group indicates that the thiophene ring is attached to the suspended amino group of carbon nitriding. In Fig. 4d, the O 1s spectra of both samples have characteristic peaks at ~ 530 eV from surface-adsorbed H_2O and at ~ 532 eV from surface-adsorbed O_2. From Fig. 4e, the S 2p spectra of CN-PTh-Br(0.5) have two characteristic peaks at 163.68 (S $2p_{3/2}$) and 165.88 eV (S $2p_{1/2}$), respectively, which are caused by the presence of Sulphur in thiophene. In the CN-PTh-Br(0.5) sample (Fig. 4f), the corresponding peaks of Br $3d_{5/2}$, and Br $3d_{3/2}$ representing the C-Br bond in PTh-Br at 67.48 and 68.58 eV were observed respectively. Therefore, combined with the above results, it can be concluded that conjugated polymer PTh-Br was grafted onto the structure of carbon nitride.

3.2. Optical and electrochemical properties

Fig. 5a displays the UV–visible diffuse reflectance spectra used to evaluate the optical properties of the photocatalysts. Two peaks appeared at approximately 260 and 380 nm could be due to π-π* or n-π* electronic transitions in the heptazine ring conjugated system.[52] The absorption edges of the PTh-Br-modified catalysts were red-shifted compared to that of CN (near 450 nm), which consequently enhanced their light absorption in the 450–600 nm range. The redshift of the absorption indicates the formation of polymers with higher conjugation lengths[53] and the redshift increases with the content of PTh-Br, which implies that the conjugated polymer PTh-Br was successfully introduced to the edges of the carbon nitride structure. It clearly states that the light-trapping ability of CN-PTh-Br(x) in the visible region is significantly enhanced, implying its potential to possess considerable photocatalytic activity. Therefore, it can be proved that the PTh-Br modification promotes the photocatalytic activity of CN-PTh-Br(x) caused by the increase in visible-light absorption capacity.

As expected, the E_g value decreases from 2.52 eV for CN to 2.28 eV for CN-PTh-Br(0.5) (Fig. 5b) according to Eq. (1):

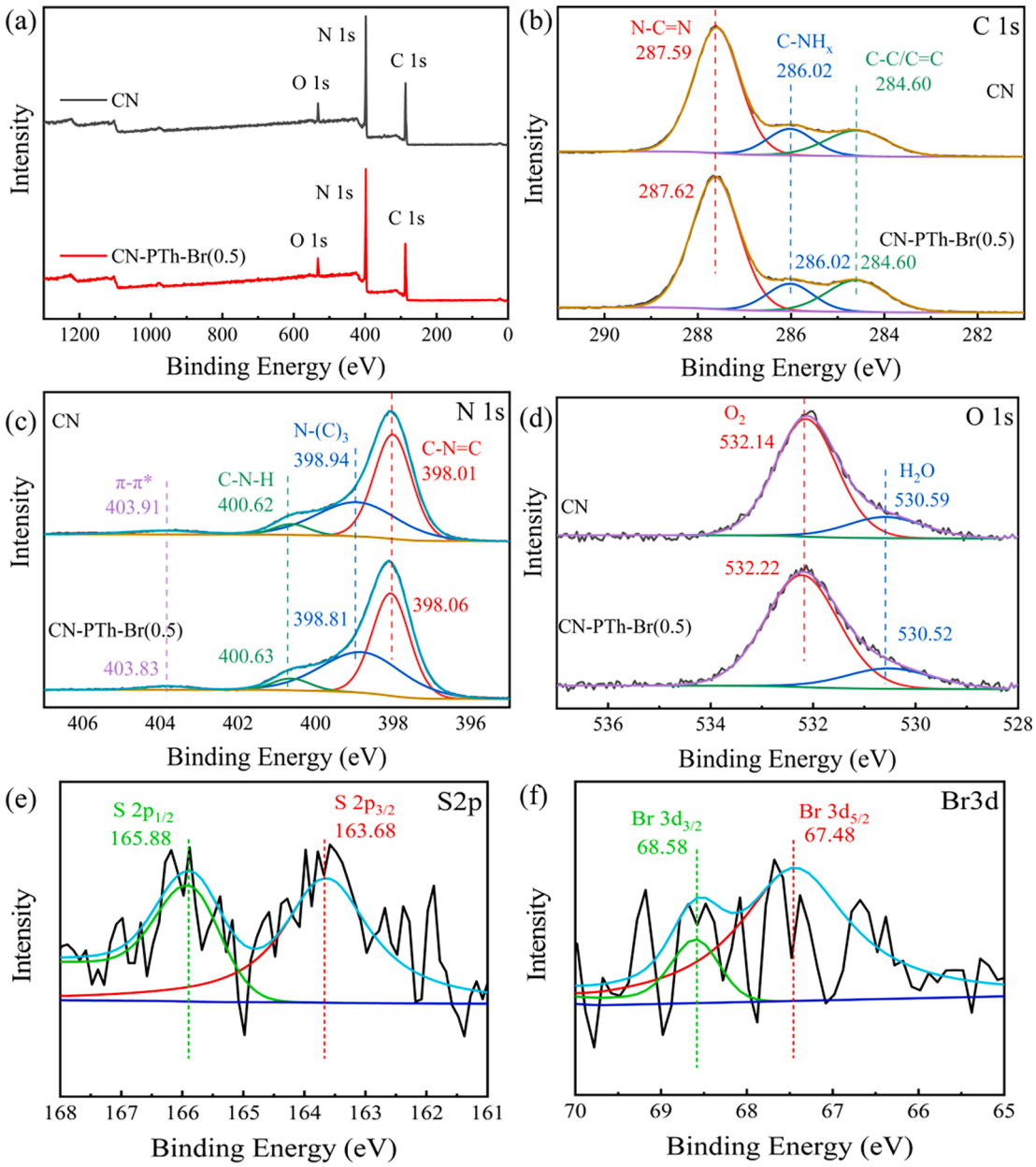

Fig. 4. (a) Full XPS spectra, high-resolution XPS spectra of (b) C 1s, (c) N 1s, and (d) O 1s of CN and CN-PTh-Br(0.5), and high-resolution XPS spectra of (e) S 2p and (f) Br 3d of CN-PTh-Br(0.5).

$$(\alpha h\nu)^{1/2} = A(h\nu - E_g) \quad (1)$$

where α represents the absorption coefficient, A denotes a constant, h is Planck constant, ν symbolizes optical frequency, and E_g signifies direct band gap energy. Modifying the carbon nitride backbone with a conjugated polymer can both optimize the electronic structure and narrow the optical band gap, while the electronegative bromine substituents on the main chain of the aforementioned conjugated polymer can also alter the charge transport properties[54], further improving the charge mobility in the process of photocatalytic redox reaction.

Fig. 5c illustrates the Mott-Schottky curves of the catalysts, both before and after modification, which have positive slopes, indicating that they are n-type semiconductors, and the modification does not change their conductive behavior.[55] Remarkably, the slope of CN-PTh-Br(0.5) becomes smaller, indicating faster carrier migration and separation. It is widely recognized for n-type semiconductors, the conduction band bottom has a potential that is ~ 0.1 V more negative compared to the flat band.[56] Therefore, the conduction band potentials of CN and CN-PTh-Br(0.5) are converted to −0.55 and −0.66 V *vs.* NHE. The E_{VB} value is calculated using Eq. (2):

$$E_{VB} = E_{CB} + E_g \quad (2)$$

where E_{VB} denotes the valence band (VB) value, and E_{CB} presents the conduction band (CB) value. The energy band structures of CN and CN-PTh-Br(0.5) are depicted in Fig. 5d, and the VB of these materials are 1.97 and 1.62 V *vs.* NHE. Following the creation of mesoporous material and the modification by PTh-Br, both the VB and CB values of CN-PTh-Br (0.5) shifted negatively, with the CB value shifted to a higher energy by 0.11 V compared to that of CN, indicating that the electrons in the CB of CN-PTh-Br(0.5) are more active. The narrower band gap, the more negative displacement of CB, and the higher conductivity of CN-PTh-Br (0.5) promote electron transfer in the photocatalytic process.

Surface photovoltage (SPV) measurement (Fig. 6) is used to characterize the separation rate of photogenerated charge carriers over CN

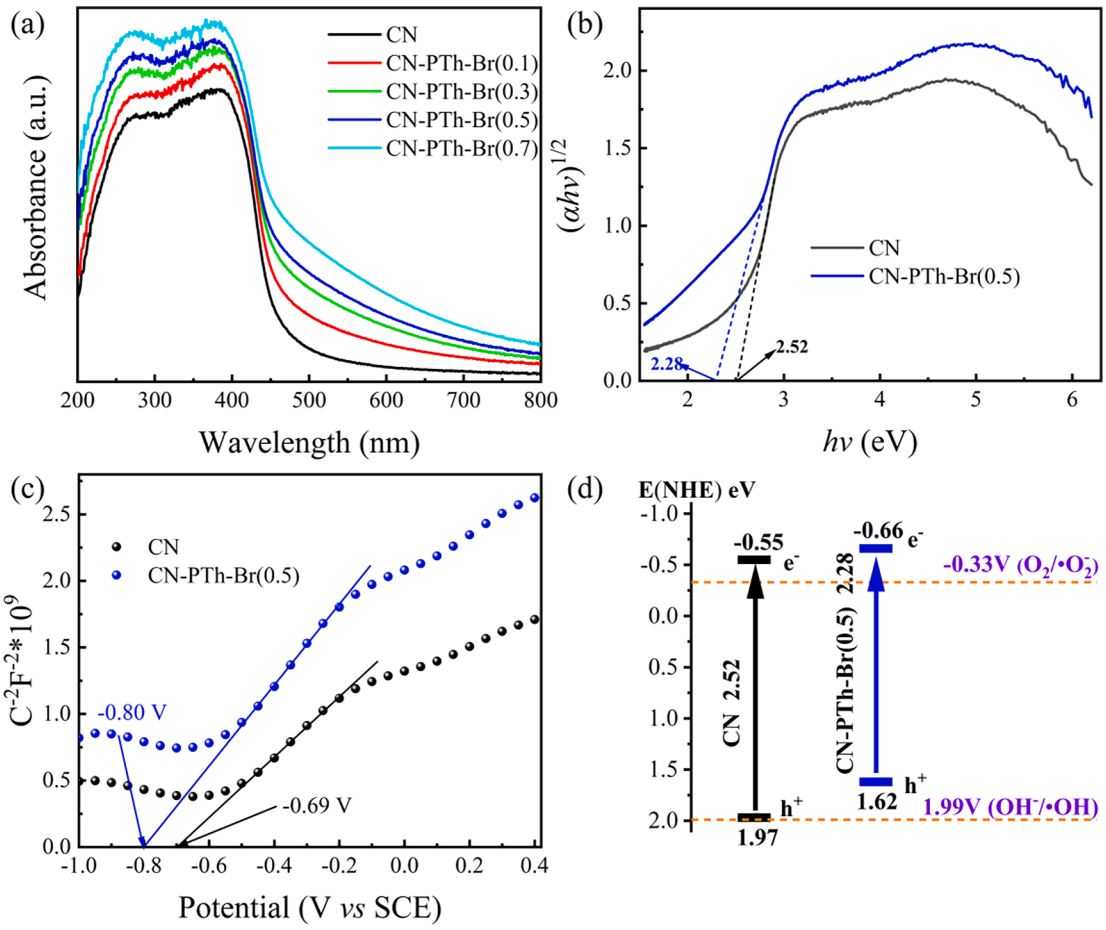

Fig. 5. (a) UV–vis diffuse reflection spectra, (b) Tauc plots, (c) Mott-Schottky curves, and (d) schematic diagram for band alignment of photocatalysts.

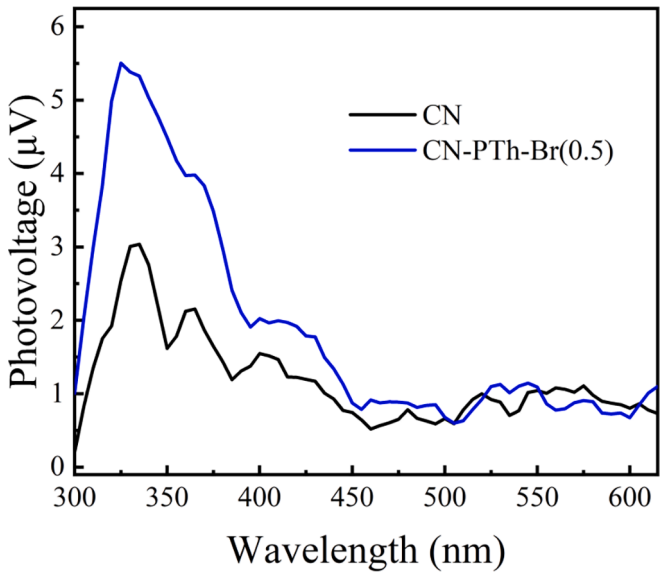

Fig. 6. Surface photovoltage (SPV) spectra of CN and CN-PTh-Br(0.5).

and CN-PTh-Br(0.5). The intensity of the SPV signal reflects the separation rate of the photoinduced electron-hole pairs. Generally, the stronger the responses of SPV spectra, the higher the charge separation. [57] The CN-PTh-Br(0.5) sample shows a stronger SPV response than CN, which reflects the greatly enhanced charge separation efficiency. Furthermore, the fluorescence spectra of the two samples were recorded to investigate their charge separation efficiency. Fig. 7a shows the photoluminescence (PL) emission spectra of photocatalysts at room temperature. With the increase of PTh-Br addition, the photoluminescence intensity of CN-PTh-Br(x) decreased gradually, and all of them were significantly lower than that of CN except CN-PTh-Br(0.1). Indeed, a higher photoluminescence intensity suggests a higher rate of carrier recombination, which in turn results in a lower photocatalytic activity. Therefore, the low emission peak intensity of CN-PTh-Br(x) suggests a superior ability to separate electrons and holes. To gain further insights into the charge carrier dynamics, a key parameter in determining the photocatalytic performance, time-resolved PL (TRPL) experiments were performed at room temperature. CN and CN-PTh-Br (0.5) were excited at 340 nm, and their emission decay curves were monitored at the maximum emission wavelength (475 nm), as shown in Fig. 7b. The average electron lifetimes are calculated by Eq. (S6). The obtained fluorescence lifetimes (τ) and their relative amplitudes (A) are summarized in Table S2. It can be known from the calculation results that the average electron lifetime (τ_{ave}) of CN is 12.38 ns, which is greater than that of CN-PTh-Br(0.5) (10.26 ns), which is ascribed to the more rapid and effective charge transfer of CN-PTh-Br(0.5).[58] The decreased average electron lifetime in the CN-PTh-Br(0.5) demonstrated a non-radiative pathway of electron interaction[59], which further suggested that the constructed D-A structure in CN-PTh-Br(0.5) served as an efficient intramolecular charge transfer channel.[31] Additionally, to assess the separation behavior of holes and electrons, photoelectrochemical trials were conducted. The transient photocurrent responses (TPR) of various catalysts are shown in Fig. 7c, which were gauged at 0 V *vs*. SCE. Under visible-light, the generated current density of CN-PTh-Br(0.5) is much higher than that of CN, indicating that CN-PTh-Br(0.5) could supply more holes and electrons engaging in the

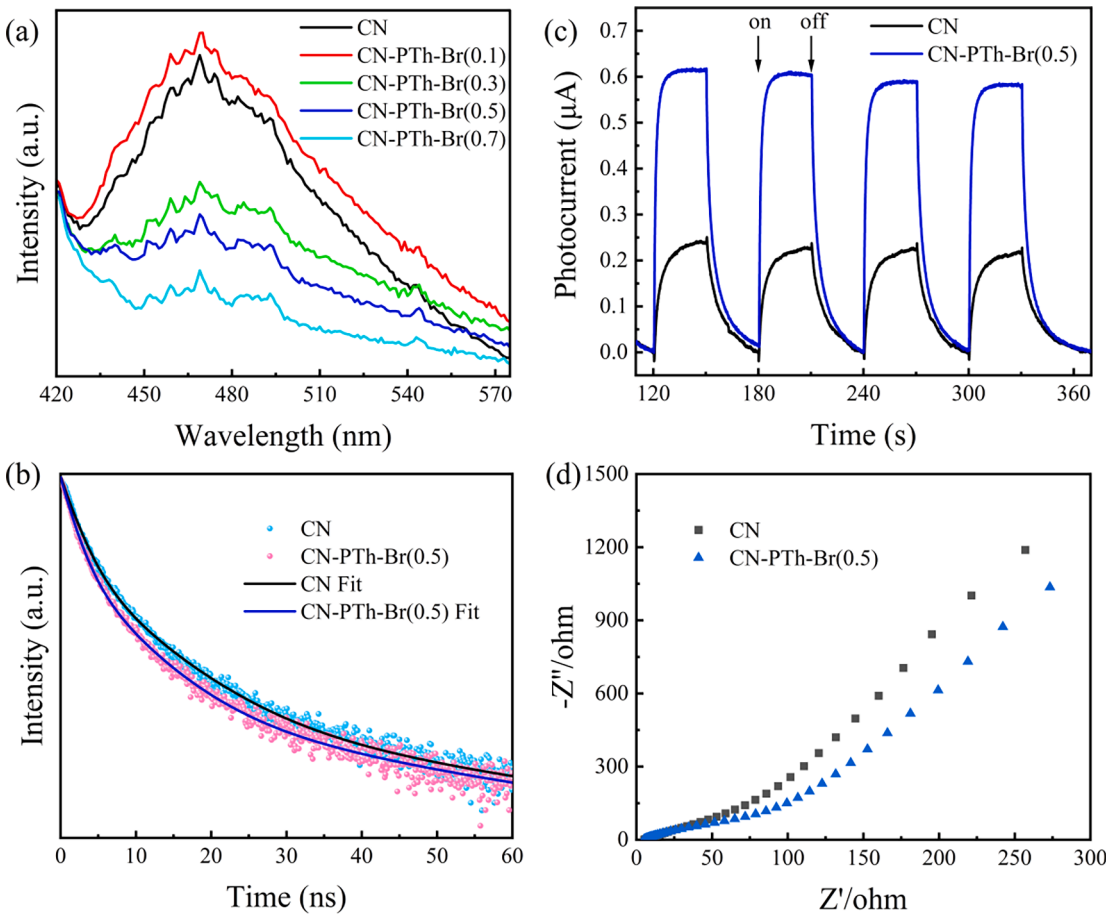

Fig. 7. (a) PL emission spectra, (b) TRPL decay spectra, (c) TPR, and (d) EIS of photocatalysts.

photocatalytic reaction process. The rapid transfer and separation of charge carriers may result from the introduction of polythiophene donors on the one hand, and the substitution of electronegative bromine on the polythiophene backbone on the other.[60,61] The arc radius of CN-PTh-Br(0.5) on the Nyquist plot from electrochemical impedance spectroscopy (EIS), as shown in Fig. 7d, was smaller than that of CN, denoting the lower transfer resistance and the higher mobility of charge. Based on these results, the polythiophene segments (electron donors) in the PTh-Br-modified carbon nitride structure can rapidly transfer electrons to the carbon nitride segments (electron acceptors), and the introduction of strongly electron-absorbing bromine atoms on the thiophene molecule can further accelerate the electron transfer, thus improving its catalytic activity.[62]

3.3. Photocatalytic activity

Fig. 8a shows a comparison of MBT photodegradation for various photocatalysts, from which it can be seen that the self-degradation of MBT and the adsorption capacity of all the samples are negligible. The degradation rates of MBT after 45 min of visible-light illumination are as follows: CN-PTh-Br(0.5) > CN-PTh-Br(1.0) > CN-PTh-Br(0.7) > CN-PTh-Br(0.3) > CN-PTh-Br(0.1) > CN. Notably, all the PTh-Br-modified catalysts significantly promoted the photocatalytic degradation of MBT, among which CN-PTh-Br(0.5) indicated the highest photocatalytic performance achieving a remarkable removal rate of 99.8%. The degradation capacity was reduced when the amount of PTh-Br used exceeded 0.5%. This decrease in photocatalytic performance could potentially be attributed to the structural distortion resulting from the introduction of excessive long-chain polythiophene, resulting in the formation of an increased number of holes and electrons complex sites. The degradation intermediate products of MBT were detected by HPLC-MS, and the mass spectrometry results are shown in Fig. S3.

The kinetic curves of MBT degradation over CN-PTh-Br(0.5) are depicted in Fig. 8b. It is obvious that two types of kinetic characteristics are shown at different degradation times, with the photocatalytic degradation data conforming to a zero-order kinetic curve in the first 20 min (Fig. 8b, left) and a first-order kinetic curve in the range of 20–30 min (Fig. 8b, right). During the first 20 min, the photodegradation reaction rate was almost independent of MBT concentration, which may be caused by the initial contaminant solution containing excessive MBT. The zero-order degradation reaction rate constant (K_0) was 0.72 mg/L min^{-1}. After 20 min of the photodegradation reaction, it was observed that the diffusion rate from the solution to the surface of the photocatalyst decreased with lower concentrations of MBT, resulting in the influence of MBT concentration at this stage cannot be ignored. The first-order degradation reaction rate constant (K_1) was 0.13 min^{-1}.

From Fig. 8c, the photocatalytic degradation data for all samples appeared to fit the zero-order kinetic curve throughout the photodegradation process. This phenomenon might be caused by the relatively lower photocatalytic degradation rate of MBT in these samples, leading to the concentration of MBT still being relatively higher within the first 30 min of photodegradation. The K_0 values of MBT over CN, CN-PTh-Br(0.1), CN-PTh-Br(0.3), CN-PTh-Br(0.7), and CN-PTh-Br(1.0) were 0.23, 0.43, 0.47, 0.50, and 0.53 mg/L min^{-1}, respectively, where the K_0 of CN-PTh-Br(0.5) was thrice that of CN. The aforementioned results reveal that CN-PTh-Br(0.5) has the highest photocatalytic degradation performance for MBT removal.

To evaluate the stability of CN-PTh-Br(0.5), five consecutive MBT degradation experiments were performed (Fig. 8d). It was evident that the photocatalytic efficiency of CN-PTh-Br(0.5) was almost unchanged

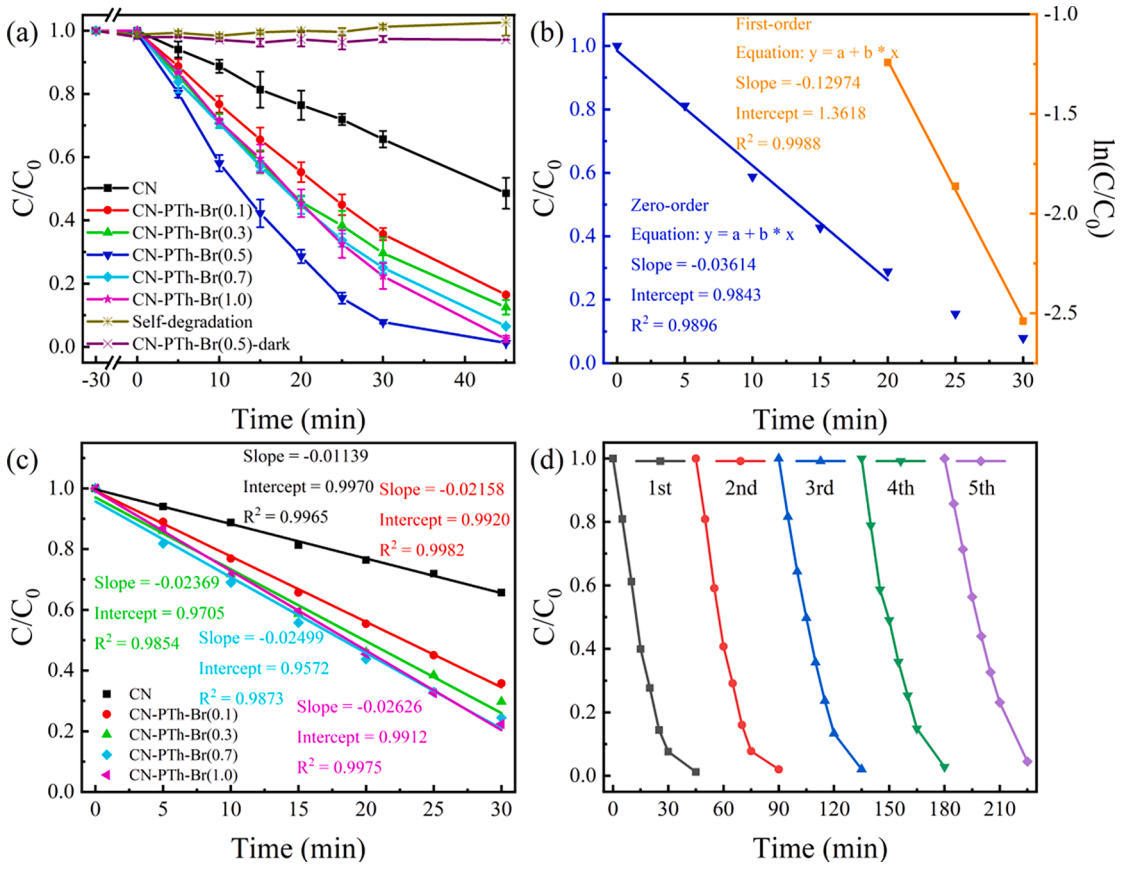

Fig. 8. (a) Photocatalytic degradation of MBT (20 mg/L) by various photocatalysts, (b) zero-order kinetic curve (left) and the first-order kinetic curve (right) of MBT degradation over CN-PTh-Br(0.5), (c) zero-order kinetic curves of MBT degradation over CN, CN-PTh-Br(0.1), CN-PTh-Br(0.3), CN-PTh-Br(0.7), and CN-PTh-Br(1.0), (d) the cycle experiments of CN-PTh-Br(0.5).

after five cycles, indicating excellent stability and reusability of the CN-PTh-Br(0.5) photocatalyst.

The actual water contains various ions, which will affect the practical application of photocatalysts. The application of the material in the real environment was simulated using actual river water. As shown in Fig. 9b, the river water was collected from the Ba River in Xi'an, Shaanxi Province China. The initial concentration of MBT is 20 mg/L, and the experimental results are displayed in Fig. 9a. The photocatalytic performance of CN-PTh-Br(0.5) in the actual river water shows a slight increase compared to that in DI water, which may be due to the small amount of humic acid in the river water. The humic acid molecules have a quinone structure and probably react with water to generate ·OH under light irradiation.[63] The CN-PTh-Br(0.5) sample shows excellent removal ability in actual water bodies, which indicates that it has great potential in wastewater treatment.

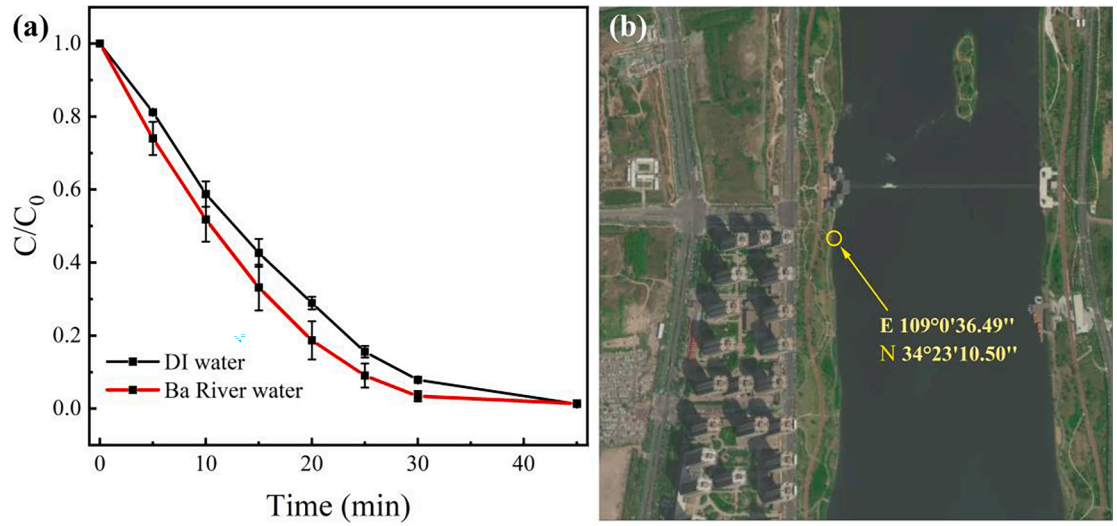

Fig. 9. (a) Effect of different water samples on the degradation of MBT over CN-PTh-Br(0.5) under visible light irradiation, (b) the water source sampling points.

3.4. Photocatalytic mechanisms

During the photocatalytic degradation of MBT over CN-PTh-Br(0.5), L-Ascorbic acid, EDTA-2Na, and TBA were selected as the scavengers for the three primary active species in the photocatalytic reaction process: $\bullet O_2^-$, h^+, and •OH.[64] From Fig. 10, compared with the experiment without any scavengers, the addition of L-Ascorbic acid completely inhibited the photo-degradation of MBT, the addition of EDTA-2Na reduced the photocatalytic removal rate of MBT by about 22%, and the addition of TBA had almost no interference on the photocatalytic removal rate of MBT. These results indicated that $\bullet O_2^-$ played the most significant role during the photodegradation of MBT, followed by h^+, while •OH has minimal impact on the degradation process.

The internal electronic structures of the catalysts were monitored via electron paramagnetic resonance (EPR). As shown in Fig. 11a, both materials exhibit only one Lorentzian paramagnetic absorption signal, at approximately $g = 2.0033$, resulting from the unpaired electrons in the sp^2-hybridized carbon atoms in the aromatic heterocyclic ring.[65] In the dark, a 3-fold increase in the EPR signal intensity was obtained for CN-PTh-Br(0.5) compared with CN. This result illustrated that with the incorporation of PTh-Br into the carbon nitride frameworks, the π electrons in the D-A structured CN-PTh-Br(0.5) were redistributed, which resulted in more intensive delocalization that might inhibit the recombination of carriers. The EPR measurements validated the PL studies, in which we observed an efficient separation of the charge.[66]

In addition, the EPR was measured to further determine the existence of reactive oxygen species in the photodegradation process using DMPO as the scavenging agent. From Fig. 11b, in the system containing CN or CN-PTh-Br(0.5) under visible-light, the characteristic signals of DMPO-$\bullet O_2^-$ were detected, which were not present in the dark, suggesting that DMPO-$\bullet O_2^-$ exists in the heterogeneous photocatalytic systems of CN or CN-PTh-Br(0.5). For both CN and CN-PTh-Br(0.5), the longer the visible-light irradiation time, the stronger the DMPO-$\cdot O_2^-$ signal intensity, and CN-PTh-Br(0.5) displays a stronger intensity for the same light irradiation time. Since the DMPO-$\cdot O_2^-$ signal intensity is proportional to the concentration of unpaired electrons, it indicates that the stronger signal intensity is more conducive to the generation of $\cdot O_2^-$ in the photocatalytic reaction, i.e., the PTh-Br-modified photocatalysts can generate photoelectrons more efficiently. The results of EPR are congruent with the active species quenching experiment.

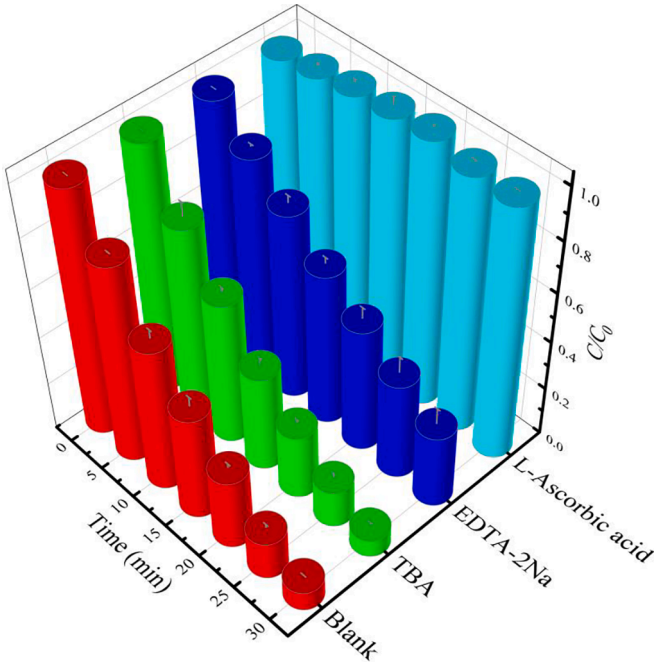

Fig. 10. The photodegradation of MBT (20 mg/L) over CN-PTh-Br(0.5) with the existence of different scavengers.

3.5. DFT calculations and possible photocatalytic mechanism

To further reveal the relationship between the enhanced photocatalytic performance and the D-A structure, the electronic band structures of CN and CN-PTh-Br(0.5) were calculated by DFT. The spatial distribution of charge density over the HOMO and LUMO is shown in Fig. 12. For the CN, the HOMO is located on the N atoms of the exocyclic ring of the heptazine ring, and the LUMO is located on the C atoms of the exocyclic ring of the heptazine ring and on the N atom of the ring center.[67] It can be inferred that the high symmetry of the planar structure in CN leads to a uniform distribution of HOMO and LUMO, which reduces the electron-hole separation. While the electron cloud of the modified CN-PTh-Br(0.5) underwent redistribution, the HOMO was mainly concentrated on the PTh-Br segment, while the LUMO was mainly concentrated on the heptazine rings connected to PTh-Br, which might be related to the fact that PTh-Br is an electron-rich group. The HOMO and LUMO of CN-PTh-Br(0.5) were separated on different areas, which verified that the newly formed D-A structures effectively separated the photogenerated electrons and holes.[59] Therefore, the PTh-Br in CN-PTh-Br(0.5) can be served as an electron donor based on the electron-donating nature of HOMO.[68] Moreover, compared to CN, the HOMO and LUMO distribution in CN-PTh-Br(0.5) is more dispersed, which is more conducive to the spatial separation of charge carriers. Intramolecular electron transfer occurs when electrons on the HOMO energy level of the donor segment are excited by visible-light and driven to the LUMO energy level of the acceptor segment, whereas the holes remain on the HOMO energy level of the donor segment. As shown in Fig. S4 and Table S3, the charge analysis indicates that the PTh-Br segment (electron donor) tends to provide electrons to heptazine rings (electron acceptor) in CN-PTh-Br(0.5), resulting in a transfer charge of 0.195 e. In addition, the introduction of PTh-Br into the carbon nitride skeleton leads to a shift in the HOMO energy level from −6.30 to −5.81 eV, and the LUMO energy level from −2.40 to −2.48 eV, causing a decrease of the energy gap by 0.57 eV, which well match to the result of UV–vis DRS (Fig. 5). The addition of conjugated PTh-Br reduced the LUMO energy level of CN-PTh-Br(0.5) by 0.08 eV compared to CN, indicating that the introduction of the electron donor had little effect on the LUMO energy level and did not inhibit the formation of the active species. Therefore, the D-A structured CN-PTh-Br(0.5) composed of electron donor PTh-Br and electron acceptor heptazine rings leads to the spatial separation of electron-hole pairs and the enhancement of photocatalytic performance. From Fig. S5, the surface electrostatic potential (ESP) distribution reveals that the electrons in the CN-PTh-Br(0.5) are redistributed after the grafting of PTh-Br. Specifically, owing to the electron donor property of PTh-Br, a small number of electrons is distributed in the PTh-Br segment, while the heptazine ring segment carries more electrons.[68] In addition, CN-PTh-Br(0.5) has a larger dipole moment (≈ 2.71 D) than CN (≈ 1.77 D), indicating that it can promote charge separation and transfer. These results support the notion that the PTh-Br structure in CN-PTh-Br(0.5) can be used as an electron donor to promote photocatalytic degradation of pollutants.

Based on all experimental results and DFT calculations, a probable mechanism of CN-PTh-Br(0.5) photocatalytic activity enhancement was proposed in Scheme. 1. As a strong electron donor, polythiophene has an extensive π-conjugated framework, which can facilitate electron-hole pairs separation and inhibit photogenerated charge carriers recombination. Under visible-light irradiation, CN-PTh-Br(0.5) produced photogenerated electrons and holes, whereas the π-electrons in the polythiophene donor tended to be transferred intramolecular to the heptazine ring in the carbon nitride acceptor via the C-N bond due to the presence of the D-A structure in CN-PTh-Br(0.5). Furthermore, the holes of carbon nitride acceptor can transfer to polythiophene donor and effectively restrain the electron-hole pairs recombination. Meanwhile,

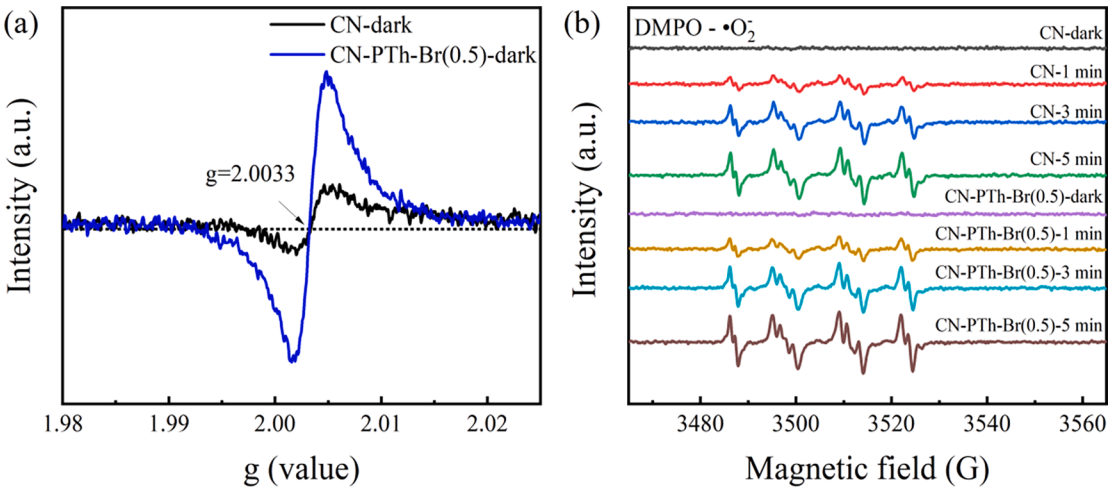

Fig. 11. EPR spectra of (a) CN and CN-PTh-Br(0.5) in the dark, and (b) DMPO-·O_2^- in the existence of CN or CN-PTh-Br(0.5).

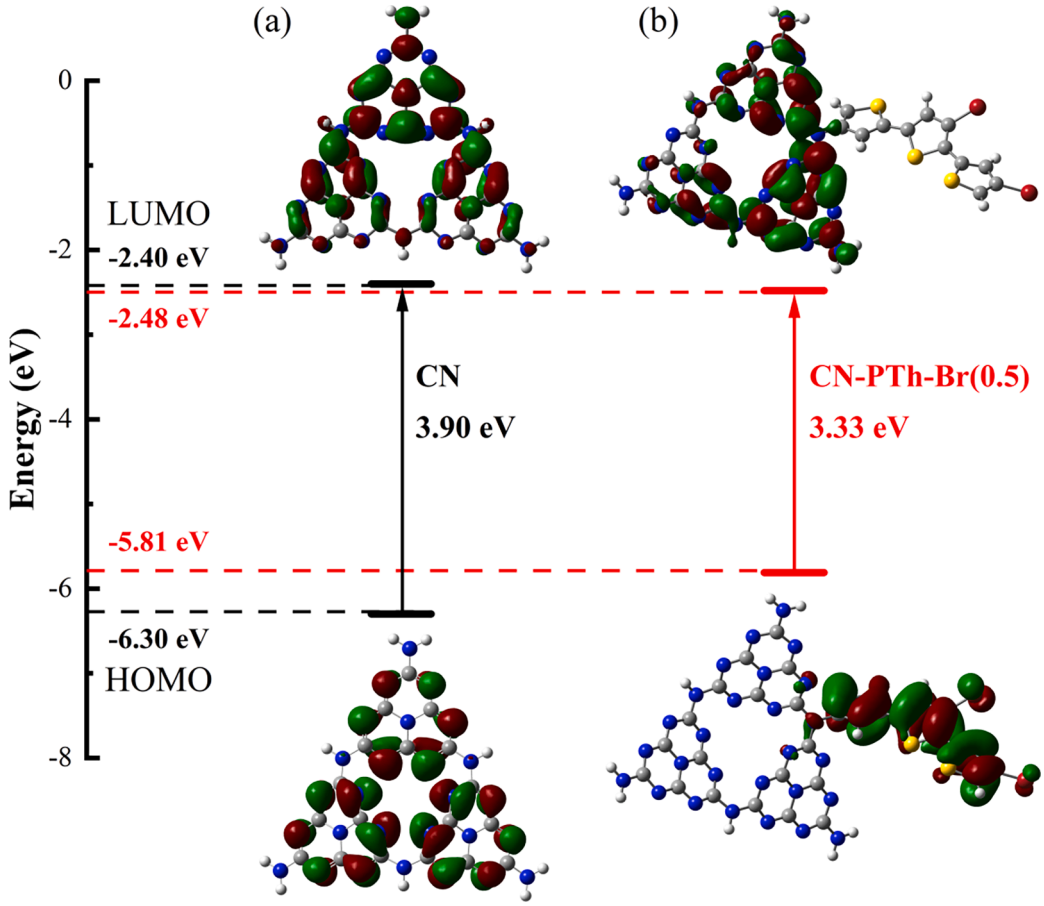

Fig. 12. Calculated HOMO energy (bottom)-LUMO energy (top) of (a) CN and (b) CN-PTh-Br(0.5).

the electrons will also competitively transfer to Br atoms caused by their own electronegative nature. The CB potential of CN-PTh-Br(0.5) (-0.66 V *vs.* NHE) is more negative than the redox potential of the oxygen/superoxide ($O_2/\cdot O_2^-$) couple, which is −0.33 V *vs.* NHE, suggesting that the electrons on CB could react with O_2 to form $\cdot O_2^-$. Indeed, introducing PTh-Br to the CN-PTh-Br(0.5) backbone decreases the CB potential of the photocatalyst, and expedites the electron transfer from CB to oxygen molecules to format $\cdot O_2^-$. In addition, the VB potential of CN-PTh-Br(0.5) (+1.62 V *vs.* NHE) is too low to oxidize OH^- to ·OH, but the holes on VB can oxidize organic pollutants directly.

4. Conclusions

In summary, a series of D-A structured CN-PTh-Br(x) photocatalysts based on polythiophene donors and carbon nitride acceptors using PTh-Br and DCD as precursors have been prepared by thermal copolymerization for the first time. Under visible-light irradiation, CN-PTh-Br(0.5) had the best photocatalytic performance and removed 99.8% of MBT in 45 min. The high photocatalytic activity of CN-PTh-Br(0.5) can be attributed to two reasons. Firstly, enhanced visible-light capture and utilization due to the long-chain nature of the conjugated polymer PTh-

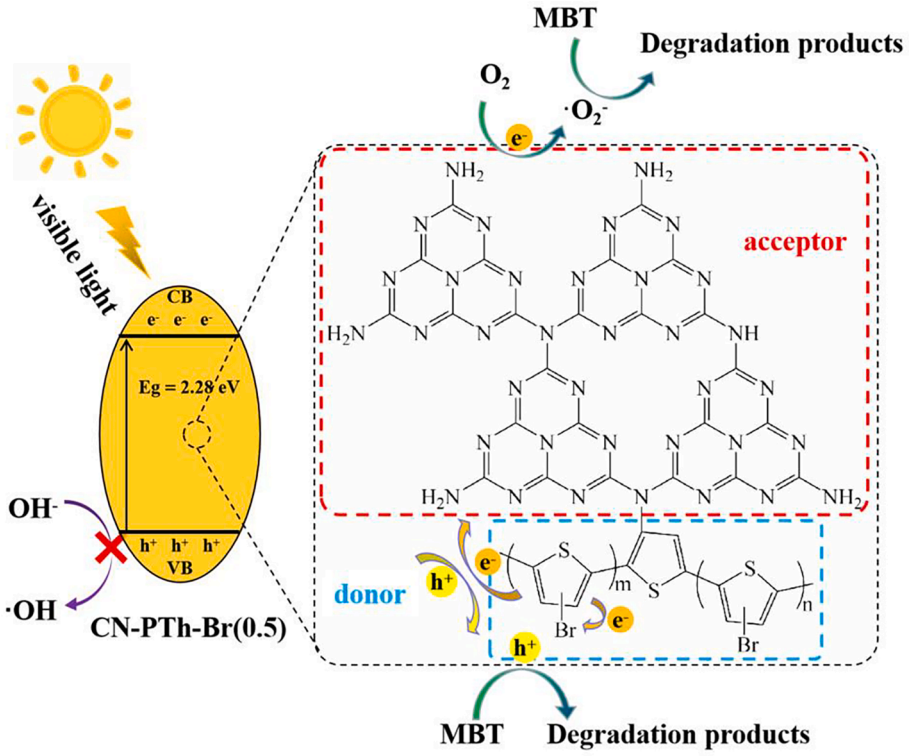

Scheme 1. Photocatalytic Degradation Mechanism over CN-PTh-Br(0.5) under Sunlight Irradiation.

Br. Secondly, the intramolecular charge transfer, formed by the introduction of electron-rich thiophene groups with negatively charged Br atoms, enables force-directed migration of electrons from thiophene segment (donor) to carbon nitride segment (acceptor) in CN-PTh-Br (0.5), which can improve the separation efficiency of electron-hole pairs and reduce the recombination of photogenerated charge carriers. Base on EPR and free radicals quenching experiments, it has been deduced that $\cdot O_2^-$ serves as the primary oxidizing species. In addition, CN-PTh-Br(0.5) shows sufficient reusability. Our research may offer a fresh approach to design composite photocatalysts with high photocatalytic activity.

CRediT authorship contribution statement

Yao Huang: Investigation, Methodology, Validation, Writing – original draft, Writing – review & editing. **Xuefeng Hu:** Conceptualization, Formal analysis, Funding acquisition, Investigation, Methodology, Supervision, Validation, Writing – review & editing. **Chuanyi Wang:** Supervision, Writing – review & editing. **Detlef Bahnemann:** Supervision, Writing – review & editing.

Declaration of competing interest

The authors declare that they have no known competing financial interests or personal relationships that could have appeared to influence the work reported in this paper.

Data availability

Data will be made available on request.

Acknowledgement

This work was financially supported by the National Natural Science Foundation of China (No. 22376132, 22176120).

Appendix A. Supplementary data

Supplementary data to this article can be found online at https://doi.org/10.1016/j.seppur.2024.126457.

References

[1] R.B. Rajput, S.N. Jamble, R.B. Kale, A review on TiO_2/SnO_2 heterostructures as a photocatalyst for the degradation of dyes and organic pollutants, J. Environ. Manage. 307 (2022) 114533, https://doi.org/10.1016/j.jenvman.2022.114533.
[2] A. Saravanan, P.S. Kumar, S. Jeevanantham, M. Anubha, S. Jayashree, Degradation of toxic agrochemicals and pharmaceutical pollutants: Effective and alternative approaches toward photocatalysis, Environ. Pollut. (2022) 118844, https://doi.org/10.1016/j.envpol.2022.118844.
[3] S.S. Bag, S. Sinha, A. Banerjee, A. Golder, Simultaneous sensing and photocatalytic degradation to free water from toxic dye pollutants for possible agricultural and household applications: Role of generated holes and hydroxyl radicals, J. Environ. Chem. Eng. 10 (2022) 108919, https://doi.org/10.1016/j.jece.2022.108919.
[4] G. Ramalingam, P. Nagapandiselvi, A. Priya, S. Rajendran, A review of graphene-based semiconductors for photocatalytic degradation of pollutants in wastewater, Chemosphere (2022) 134391, https://doi.org/10.1016/j.chemosphere.2022.134391.
[5] M. Amanulla, C.M. Magdalane, G. Ramalingam, R. Sundaram, N. Tamam, H. Somaily, M. Al-Buriahi, Fabrication and characterization of $Th(MoO_4)_2/TiO_2$ nanocomposite for potential use in photocatalytic degradation of toxic pollutants, Appl. Phys. A 128 (2022) 397, https://doi.org/10.1007/s00339-022-05504-1.
[6] G. Ramalingam, R. Pachaiappan, P.S. Kumar, S. Dharani, S. Rajendran, D.-V.-N. Vo, T.K. Hoang, Hybrid metal organic frameworks as an Exotic material for the photocatalytic degradation of pollutants present in wastewater: a review, Chemosphere 288 (2022) 132448, https://doi.org/10.1016/j.chemosphere.2021.132448.
[7] Y.K. Manea, A.M. Khan, A.A. Wani, A.A. Saeed, S.M. Kasim, A. Mashrai, Green Water Treatment for Organic Pollutions: Photocatalytic Degradation Approach, Green Chem. Sustainable Water Purification (2023) 107–127, https://doi.org/10.1002/9781119852322.ch5.
[8] F. Zhang, X. Li, X. Dong, H. Hao, X. Lang, Thiazolo [5, 4-d] thiazole-based covalent organic framework microspheres for blue light photocatalytic selective oxidation of amines with O_2, Chin. J. Catal. 43 (2022) 2395–2404, https://doi.org/10.1016/S1872-2067(22)64127-5.
[9] F. Huang, Y. Wang, X. Dong, X. Lang, Merging benzotrithiophene covalent organic framework photocatalysis with TEMPO for selective oxidation of organic sulfides, Sci. China Chemi. 66 (2023) 3290–3296, https://doi.org/10.1007/s11426-023-1644-x.

[10] A. Kumar, P. Raizada, A. Hosseini-Bandegharaei, V.K. Thakur, V.-H. Nguyen, P. Singh, C-, N-Vacancy defect engineered polymeric carbon nitride towards photocatalysis: viewpoints and challenges, J. Mater. Chem. A 9 (2021) 111–153, https://doi.org/10.1039/D0TA08384D.

[11] J. Yuan, X. Liu, Y. Tang, Y. Zeng, L. Wang, S. Zhang, T. Cai, Y. Liu, S. Luo, Y. Pei, Positioning cyanamide defects in g-C_3N_4: engineering energy levels and active sites for superior photocatalytic hydrogen evolution, Appl Catal B 237 (2018) 24–31, https://doi.org/10.1016/j.apcatb.2018.05.064.

[12] Z. Chen, S. Zhang, Y. Liu, N.S. Alharbi, S.O. Rabah, S. Wang, X. Wang, Synthesis and fabrication of g-C_3N_4-based materials and their application in elimination of pollutants, Sci. Total Environ. 731 (2020) 139054, https://doi.org/10.1016/j.scitotenv.2020.139054.

[13] L. Yang, X. Liu, Z. Liu, C. Wang, G. Liu, Q. Li, X. Feng, Enhanced photocatalytic activity of g-C_3N_4 2D nanosheets through thermal exfoliation using dicyandiamide as precursor, Ceram. Int. 44 (2018) 20613–20619, https://doi.org/10.1016/j.ceramint.2018.06.105.

[14] W. Yang, L. Jia, P. Wu, H. Zhai, J. He, C. Liu, W. Jiang, Effect of thermal program on structure-activity relationship of g-C_3N_4 prepared by urea pyrolysis and its application for controllable production of g-C_3N_4, J. Solid State Chem. 304 (2021) 122545, https://doi.org/10.1016/j.jssc.2021.122545.

[15] Y. Yi, J. Wang, Y. Niu, Y. Yu, S. Wu, K. Ding, Exploring the evolution patterns of melem from thermal synthesis of melamine to graphitic carbon nitride, RSC Adv. 12 (2022) 24311–24318, https://doi.org/10.1039/D2RA03337B.

[16] Y. Wang, G. Tan, M. Dang, S. Dong, Y. Liu, T. Liu, H. Ren, A. Xia, L. Lv, Study on surface modification of g-C_3N_4 photocatalyst, J. Alloy. Compd. 908 (2022) 164507, https://doi.org/10.1016/j.jallcom.2022.164507.

[17] N.S.N. Hasnan, M.A. Mohamed, Z.A. Mohd Hir, Surface Physicochemistry Modification and Structural Nanoarchitectures of g-C_3N_4 for Wastewater Remediation and Solar Fuel Generation, Adv. Mater. Technol. 7 (2022) 2100993, https://doi.org/10.1002/admt.202100993.

[18] K. Xu, K. Cui, M. Cui, X. Liu, X. Chen, X. Tang, X. Wang, Electronic structure modulation of g-C_3N_4 by Hydroxyl-grafting for enhanced photocatalytic peroxymonosulfate Activation: Combined experimental and theoretical analysis, Sep. Purif. Technol. 294 (2022) 121246, https://doi.org/10.2139/ssrn.4067331.

[19] K. Li, D. Zhao, Y. Li, S. Luo, Z. Zhou, The synergistic photocatalytic effects of surface-modified g-C_3N_4 in simple and complex pollution systems based on a macro-thermodynamic model, Environ. Sci. Nano 8 (2021) 217–232, https://doi.org/10.1039/D0EN00759E.

[20] M. Arumugam, M. Tahir, P. Praserthdam, Effect of nonmetals (B, O, P, and S) doped with porous g-C_3N_4 for improved electron transfer towards photocatalytic CO_2 reduction with water into CH_4, Chemosphere 286 (2022) 131765, https://doi.org/10.1016/j.chemosphere.2021.131765.

[21] S. Balu, Y.-L. Chen, S.-W. Chen, T.-C.-K. Yang, Rational synthesis of BixFe1-xVO_4 heterostructures impregnated sulfur-doped g-C_3N_4: A visible-light-driven type-II heterojunction photo (electro) catalyst for efficient photodegradation of roxarsone and photoelectrochemical OER reactions, Appl Catal B 304 (2022) 120852, https://doi.org/10.1016/j.apcatb.2021.120852.

[22] T. Luo, X. Hu, Z. She, J. Wei, X. Feng, F. Chang, Synergistic effects of Ag-doped and morphology regulation of graphitic carbon nitride nanosheets for enhanced photocatalytic performance, J. Mol. Liq. 324 (2021) 114772, https://doi.org/10.1016/j.molliq.2020.114772.

[23] C. Yang, X. Hu, Y. Huang, B. Liu, J. Yang, Pyrrole nitrogen coordinated Fe on carbon nitride mediated singlet oxygen formation for efficient degradation of 2-mercaptobenzothiazole, J. Environ. Chem. Eng. 11 (2023) 109694, https://doi.org/10.1016/j.jece.2023.109694.

[24] Y. Li, Z. Xia, Q. Yang, L. Wang, Y. Xing, Review on g-C_3N_4-based S-scheme heterojunction photocatalysts, J. Mater. Sci. Technol. (2022), https://doi.org/10.1016/j.jmst.2022.02.035.

[25] Z. Liu, Y. Liu, X. Sun, H. Ji, W. Liu, Z. Cai, Construction of Z-scheme Ag/$AgVO_3$/carbon-rich g-C_3N_4 heterojunction for enhanced photocatalytic degradation of sulfamethiadiazole: DFT calculation and mechanism study, Chem. Eng. J. 433 (2022) 133604, https://doi.org/10.1016/j.cej.2021.133604.

[26] C. Zhang, M. Jia, Z. Xu, W. Xiong, Z. Yang, J. Cao, H. Peng, H. Xu, Y. Xiang, Y. Jing, Constructing 2D/2D N-ZnO/g-C_3N_4 S-scheme heterojunction: Efficient photocatalytic performance for norfloxacin degradation, Chem. Eng. J. 430 (2022) 132652, https://doi.org/10.1016/j.cej.2021.132652.

[27] A.V. Emeline, A.V. Rudakova, R.V. Mikhaylov, V.K. Ryabchuk, N. Serpone, Electron transfer processes in heterostructured photocatalysts, in: Springer Handbook of Inorganic Photochemistry, Springer, 2022, pp. 73–104.

[28] C. Zhu, T. Wei, Y. Wei, L. Wang, M. Lu, Y. Yuan, L. Yin, L. Huang, Unravelling intramolecular charge transfer in donor–acceptor structured g-C_3N_4 for superior photocatalytic hydrogen evolution, J. Mater. Chem. A 9 (2021) 1207–1212, https://doi.org/10.1039/d0ta08609f.

[29] H. Che, C. Liu, G. Che, G. Liao, H. Dong, C. Li, N. Song, C. Li, Facile construction of porous intramolecular g-C_3N_4-based donor-acceptor conjugated copolymers as highly efficient photocatalysts for superior H_2 evolution, Nano Energy 67 (2020) 104273, https://doi.org/10.1016/j.nanoen.2019.104273.

[30] X. Wu, D. Li, Y. Huang, B. Chen, B. Luo, H. Shen, M. Wang, T. Yu, W. Shi, Construction of binary donor-acceptor conjugated copolymer in g-C_3N_4 for enhanced visible light-induced hydrogen evolution, Appl. Surf. Sci. 565 (2021) 150012, https://doi.org/10.1016/j.apsusc.2021.150012.

[31] C. Zhang, Z. Ouyang, Y. Yang, X. Long, L. Qin, W. Wang, Y. Zhou, D. Qin, F. Qin, C. Lai, Molecular engineering of donor-acceptor structured g-C_3N_4 for superior photocatalytic oxytetracycline degradation, Chem. Eng. J. 448 (2022) 137370, https://doi.org/10.1016/j.cej.2022.137370.

[32] S. Wang, G. Zuo, J. Kim, H. Sirringhaus, Progress of conjugated polymers as emerging thermoelectric materials, Prog. Polym. Sci. (2022) 101548, https://doi.org/10.1016/j.progpolymsci.2022.101548.

[33] N. Luo, P. Ren, Y. Feng, X. Shao, H.-L. Zhang, Z. Liu, Side-chain engineering of conjugated polymers for high-performance organic field-effect transistors, J. Phys. Chem. Lett. 13 (2022) 1131–1146, https://doi.org/10.1021/acs.jpclett.1c03909.

[34] A. Hayat, F. Raziq, M. Khan, I. Ullah, M.U. Rahman, W.U. Khan, J. Khan, A. Ahmad, Visible-light enhanced photocatalytic performance of polypyrrole/g-C_3N_4 composites for water splitting to evolve H_2 and pollutants degradation, J. Photochem. Photobiol. A Chem. 379 (2019) 88–98, https://doi.org/10.1016/j.jphotochem.2019.05.011.

[35] Q. Li, D. Xu, J. Guo, X. Ou, F. Yan, Protonated g-C_3N_4@ polypyrrole derived N-doped porous carbon for supercapacitors and oxygen electrocatalysis, Carbon 124 (2017) 599–610, https://doi.org/10.1016/j.carbon.2017.09.029.

[36] S. Munusamy, K. Sivaranjan, P. Sabhapathy, V. Narayanan, F. Mohammad, S. Sagadevan, Enhanced electrochemical and photocatalytic activity of g-C_3N_4-PANI-PPy nanohybrids, Synth. Met. 272 (2021) 116669, https://doi.org/10.1016/j.synthmet.2020.116669.

[37] S. Hu, L. Ma, H. Wang, L. Zhang, Y. Zhao, G. Wu, Properties and photocatalytic performance of polypyrrole and polythiophene modified g-C_3N_4 nanocomposites, RSC Adv. 5 (2015) 31947–31953, https://doi.org/10.1039/C5RA02883C.

[38] R. Peymanfar, A. Mohammadi, S. Javanshir, Preparation of graphite-like carbon nitride/polythiophene nanocomposite and investigation of its optical and microwave absorbing characteristics, Compos. Commun. 21 (2020) 100421, https://doi.org/10.1016/j.coco.2020.100421.

[39] M. Luo, H. Gong, W. Yang, F. He, Y. Cao, Y. Zhang, Y. Zhang, K. Liu, H. Cao, H. Yan, Composite of g-C_3N_4 and poly (3-hexylthiophene) prepared by polymerizing thiophene-3-acetic acid treated g-C_3N_4 and 3-hexylthiophene for enhanced photocatalytic hydrogen production, Int. J. Hydrogen Energy 44 (2019) 7108–7117, https://doi.org/10.1016/j.ijhydene.2019.01.244.

[40] Y. Wang, X. Zhao, Y. Tian, Y. Wang, A.K. Jan, Y. Chen, Facile Electrospinning Synthesis of Carbonized Polyvinylpyrrolidone (PVP)/g-C_3N_4 Hybrid Films for Photoelectrochemical Applications, Chem. – European J. 23 (2017) 419–426, https://doi.org/10.1002/chem.201604468.

[41] L. Zhou, G. Xue, Electrochemical synthesis of free-standing poly (3-bromothiophene) films, Synth. Met. 87 (1997) 193–195, https://doi.org/10.1016/s0379-6779(97)80107-5.

[42] M.E. Frisch, G. Trucks, H. Schlegel, G. Scuseria, M. Robb, J. Cheeseman, G. Scalmani, V. Barone, G. Petersson, H. Nakatsuji, Gaussian 16, revision C. 01, in, Gaussian, Inc., Wallingford CT, 2016.

[43] R. Dennington, T.A. Keith, J.M. Millam, GaussView 6.0.16, Semichem Inc.: Shawnee Mission, KS, USA, (2016) 143-150.

[44] F. Liu, Y. Tong, C. Li, X. Liu, One-Dimensional Conjugated Carbon Nitrides: Synthesis and Structure Determination by HRTEM and Solid-State NMR, J. Phys. Chem. Lett. 12 (2021) 10359–10365, https://doi.org/10.1021/acs.jpclett.1c02994.

[45] H.Y. Yuan, J.Y. Bai, B. Xu, X.Y. Li, S.Y. Xiao, P.F. Liu, X.L. Wang, H.G. Yang, Graphite carbon nitride doped with a benzene ring for enhanced photocatalytic H_2 evolution, Chem. Commun. 57 (2021) 3042–3045, https://doi.org/10.1039/D0CC08345C.

[46] S. Samanta, R. Yadav, A. Kumar, A.K. Sinha, R. Srivastava, Surface modified C, O co-doped polymeric g-C_3N_4 as an efficient photocatalyst for visible light assisted CO_2 reduction and H_2O_2 production, Appl Catal B 259 (2019) 118054, https://doi.org/10.1016/J.APCATB.2019.118054.

[47] Y. Chen, Y. Qu, X. Zhou, D. Li, P. Xu, J. Sun, Phenyl-bridged graphitic carbon nitride with a porous and hollow sphere structure to enhance dissociation of photogenerated charge carriers and visible-light-driven H_2 generation, ACS Appl. Mater. Interfaces 12 (2020) 41527–41537, https://doi.org/10.1021/acsami.0c11578.

[48] W. Wu, Z. Ruan, J. Li, Y. Li, Y. Jiang, X. Xu, D. Li, Y. Yuan, K. Lin, In situ preparation and analysis of bimetal Co-doped mesoporous graphitic carbon nitride with enhanced photocatalytic activity, Nano-Micro Letters 11 (2019) 1–16, https://doi.org/10.1007/s40820-018-0236-y.

[49] Y. Wang, Y. Di, M. Antonietti, H. Li, X. Chen, X. Wang, Excellent visible-light photocatalysis of fluorinated polymeric carbon nitride solids, Chem. Mater. 22 (2010) 5119–5121, https://doi.org/10.1021/cm1019102.

[50] C. Zhao, Q. Li, Y. Xie, L. Zhang, X. Xiao, D. Wang, Y. Jiao, C.A.H. Price, B. Jiang, J. Liu, Three-dimensional assemblies of carbon nitride tubes as nanoreactors for enhanced photocatalytic hydrogen production, J. Mater. Chem. A 8 (2020) 305–312, https://doi.org/10.1039/C9TA10688J.

[51] N. Tian, H. Huang, S. Wang, T. Zhang, X. Du, Y. Zhang, Facet-charge-induced coupling dependent interfacial photocharge separation: a case of BiOI/g-C_3N_4 p-n junction, Appl Catal B 267 (2020) 118697, https://doi.org/10.1016/j.apcatb.2020.118697.

[52] H. Dai, X. Gao, E. Liu, Y. Yang, W. Hou, L. Kang, J. Fan, X. Hu, Synthesis and characterization of graphitic carbon nitride sub-microspheres using microwave method under mild condition, Diam. Relat. Mater. 38 (2013) 109–117, https://doi.org/10.1016/j.diamond.2013.06.012.

[53] Y. Huang, B. Lu, J. Xu, G. Zhu, S. Chen, R. Yue, Novel redox-active polycarbazole-functionalized polycatechol network films produced by controlled electropolymerization, J. Appl. Polym. Sci. 126 (2012) 1613–1622, https://doi.org/10.1002/app.36670.

[54] J. Yin, K. Chaitanya, X.-H. Ju, Bromination and cyanation for improving electron transport performance of anthra-tetrathiophene, J. Mater. Res. 31 (2016) 337–347, https://doi.org/10.1557/jmr.2016.8.

[55] Y.S. Jun, E.Z. Lee, X. Wang, W.H. Hong, G.D. Stucky, A. Thomas, From melamine-cyanuric acid supramolecular aggregates to carbon nitride hollow spheres, Adv. Funct. Mater. 23 (2013) 3661–3667, https://doi.org/10.1002/adfm.201203732.
[56] A. Ishikawa, T. Takata, J.N. Kondo, M. Hara, H. Kobayashi, K. Domen, Oxysulfide $Sm_2Ti_2S_2O_5$ as a stable photocatalyst for water oxidation and reduction under visible light irradiation ($\lambda \leq$ 650 nm), J. Am. Chem. Soc. 124 (2002) 13547–13553, https://doi.org/10.1021/ja0269643.
[57] C. Yang, S. Wan, B. Zhu, J. Yu, S. Cao, Calcination-regulated Microstructures of Donor-Acceptor Polymers towards Enhanced and Stable Photocatalytic H_2O_2 Production in Pure Water, Angew. Chem. 134 (2022) e202208438.
[58] H. Sun, F. Guo, J. Pan, W. Huang, K. Wang, W. Shi, One-pot thermal polymerization route to prepare N-deficient modified g-C_3N_4 for the degradation of tetracycline by the synergistic effect of photocatalysis and persulfate-based advanced oxidation process, Chem. Eng. J. 406 (2021) 126844, https://doi.org/10.1016/j.cej.2020.126844.
[59] Z. Wang, X. Zheng, P. Chen, D. Li, Q. Zhang, H. Liu, J. Zhong, W. Lv, G. Liu, Synchronous construction of a porous intramolecular D-A conjugated polymer via electron donors for superior photocatalytic decontamination, J. Hazard. Mater. 424 (2022) 127379, https://doi.org/10.1016/j.jhazmat.2021.127379.
[60] B. Peng, S. Zhang, S. Yang, H. Wang, H. Yu, S. Zhang, F. Peng, Synthesis and characterization of g-C_3N_4/Cu_2O composite catalyst with enhanced photocatalytic activity under visible light irradiation, Mater. Res. Bull. 56 (2014) 19–24, https://doi.org/10.1016/j.materresbull.2014.04.042.
[61] K. Li, Y. Jiang, W. Rao, Y. Li, X. Liu, J. Zhang, X. Xu, K. Lin, Cooperative coupling strategy for constructing 0D/2D carbon nitride composites with strengthened chemical interaction for enhanced photocatalytic applications, Chem. Eng. J. 431 (2022) 134075, https://doi.org/10.1016/j.cej.2021.134075.
[62] J. Fu, Q. Xu, J. Low, C. Jiang, J. Yu, Ultrathin 2D/2D WO_3/g-C_3N_4 step-scheme H_2-production photocatalyst, Appl Catal B 243 (2019) 556–565, https://doi.org/10.1016/j.apcatb.2018.11.011.
[63] Z. Chen, J. Jin, X. Song, G. Zhang, S. Zhang, Redox conversion of arsenite and nitrate in the UV/quinone systems, Environ. Sci. Tech. 52 (2018) 10011–10018, https://doi.org/10.1021/acs.est.8b03538.
[64] L. Shi, L. Liang, J. Ma, J. Sun, Improved photocatalytic performance over AgBr/ZnO under visible light, Superlattice. Microst. 62 (2013) 128–139, https://doi.org/10.1016/j.spmi.2013.07.013.
[65] Y. Che, Q. Liu, B. Lu, J. Zhai, K. Wang, Z. Liu, Plasmonic ternary hybrid photocatalyst based on polymeric g-C_3N_4 towards visible light hydrogen generation, Sci. Rep. 10 (2020) 721, https://doi.org/10.1038/s41598-020-57493-x.
[66] C. Li, T. Zhou, M. Yan, S. Cheng, Y. Wang, J. Sun, G. Chen, H. Dong, Intramolecular π-conjugated channel expansion achieved by doping cross-linked dopants into carbon nitride frameworks for propelling photocatalytic hydrogen evolution and mechanism insight, Inorg. Chem. Front. 9 (2022) 60–69, https://doi.org/10.1039/D1QI01122G.
[67] B. Wei, J. Luo, S. Lin, Z. Li, X. Zhu, Z. Dong, S. Xiao, X. Cao, Y. Liu, Z. Zhang, Exciton dissociation and electron transfer behavior of a novel Donor-Acceptor g-C_3N_4 organic semiconductor photocatalytic separation of uranium, Sep. Purif. Technol. 318 (2023) 123918, https://doi.org/10.1016/j.seppur.2023.123918.
[68] Q. Zhang, J. Chen, X. Gao, H. Che, P. Wang, B. Liu, Y. Ao, Enhanced photocatalytic degradation of bisphenol A by a novel donor–acceptor g-C_3N_4: π-π interactions boosting the adsorption and electron transfer behaviors, Sep. Purif. Technol. 300 (2022) 121947, https://doi.org/10.1016/j.seppur.2022.121947.